Applied Catalysis B: Environmental 99 (2010) 329–335

Contents lists available at ScienceDirect

Applied Catalysis B: Environmental

journal homepage: www.elsevier.com/locate/apcatb

Photocatalysis of gas-phase toluene using silica–titania composites: Performance of a novel catalyst immobilization technique suitable for large-scale applications

Christina Akly*, Paul A. Chadik, David W. Mazyck

Department of Environmental Engineering Sciences, University of Florida, P.O. Box 116450, Gainesville, FL 32611, United States

ARTICLE INFO

Article history:
Received 15 April 2010
Received in revised form 13 June 2010
Accepted 1 July 2010
Available online 13 July 2010

Keywords:
Photocatalysis
Toluene
Titanium dioxide
Silica–titania composites
Annular reactor

ABSTRACT

Nanostructured silica–titania composites (STCs) were casted as large cylindrical pellets to be used in an annular packed-bed reactor. Their performance for the photocatalytic conversion of toluene was investigated as a function of relative humidity (RH) and space time. The 172 Å STCs were analyzed for their titania surface area (SA) available for reaction. Using silica as the titania support resulted in a loss of available titania SA of about 20%. However, casting the STCs in a large cylindrical pellet shape did not seem to further decrease the available titania SA. The effect of RH in the conversion of toluene was very significant. By increasing the RH from 13% to 90%, the conversion of toluene increased by 57%. Despite the large increase in RH, the catalyst still showed the yellowish coloration found at low RH, which is usually associated with deactivation. Toluene conversion increased with space time and steady-state conversions as high as 93% were achieved by increasing the space time up to 25 s. For all conditions studied neither external nor internal mass transfer resistances were found to be significant. The pseudo-first-order kinetics equation was successfully fit to the data and resulted in a rate constant of 0.12 s^{-1}.

1. Introduction

Many volatile organic compounds (VOCs) are currently regulated as air contaminants because of the threat they pose to human health and the environment. VOCs can be involved in the production of photochemical oxidants such as ozone which can be toxic to humans when present in the troposphere; they can be implicated in acid rain formation and the depletion of stratospheric ozone [1]. Due to their known adverse effects and their extensive use indoors and in many industrial processes, emissions of VOCs from different mobile and stationary sources are being more strictly regulated. Recently, for example, the U.S. Environmental Protection Agency published a proposed rule to lower the current primary and secondary ambient air quality standards for ozone [2]. As a consequence, the implementation of stringer regulations on VOCs emissions is expected due to their direct implication with ozone formation.

Numerous treatment technologies have been developed to remove VOCs from the environment. Unlike most conventional treatment technologies for VOCs that simply transfer the contaminants to other phases, heterogeneous photocatalysis using titanium dioxide (TiO_2) has received increased attention over the past decades because it has the potential to completely mineralize VOCs to CO_2 and water, it does not require high operating temperatures and the catalyst is continuously self-regenerating, thus eliminating catalyst replacement and sorbent disposal issues. One of the major drawbacks of using titanium dioxide, namely the commercially available form known as Degussa P25, for the photocatalytic oxidation (PCO) of gas-phase VOCs is the difficulty of immobilizing the catalyst. Commonly used techniques for catalyst immobilization include coating of the reactor walls or coating of other materials such as glass fibers or aluminum films [3,4]. Thin-film coating of reactor walls allows for high UV radiation per surface area but tends to be impractical for large-scale applications since the area coated is directly related to the size of the reactor. Furthermore, the durability of the coating might be questionable for large-scale operations since thin films tend to be easily detached from the coated surfaces. Fixed bed reactors are a better option for large-scale implementation but finding suitable packing material can be challenging. Coating of typical packing materials such as Raschig rings can improve the surface area of the catalyst available

* Corresponding author. Present address: 2107 E Foster Dr, Ada, OK 74820, United States. Tel.: +1 352 562 9524.
E-mail addresses: aklychristina@gmail.com (C. Akly), pchadik@ufl.edu (P.A. Chadik), dmazyck@ufl.edu (D.W. Mazyck).

0926-3373/$ – see front matter © 2010 Elsevier B.V. All rights reserved.
doi:10.1016/j.apcatb.2010.07.002

per volume of reactor [5], but it does not address the issue related to coating durability.

Consequently, in this work, nanostructured silica–titania composites (STCs) were synthesized and casted in a cylindrical pellet shape to be used in a packed-bed reactor. Silica supports can be advantageous over other supports due to their moderately large surface area available for adsorption, controllable pore size and narrow pore size distribution. Enhanced adsorption can be beneficial for PCO since it can bring the contaminant closer to the active sites and provide more time for the surface reactions to take place [6–8]. Although silica supports have been used by other authors to immobilize titania, the composite is usually coated to other surfaces [6,7] and not casted as large pellets to be used as the reactor packing itself, as is the case in this work.

STCs prepared using a similar formulation to the one used in this study have been previously tested for the removal of methanol and steady-state conversions higher than 95% were reported [9,10]. Although high conversions have been reported for many classes of VOCs including alcohols and chlorinated compounds during PCO using TiO_2, aromatic compounds such as toluene and benzene have usually shown high initial conversions (>60%) followed by very low steady-state conversions (<20%) attributed to catalyst deactivation under a wide range of conditions [11]. A major factor reported to influence the conversion of toluene and the extent of catalyst deactivation is the level of water vapor present in the influent air stream [11]. Obee and Brown [12] showed that the effect of water vapor on toluene oxidation rates in the process stream is dependent on the influent toluene concentration. At low toluene concentrations (<3 ppm_v), increasing the levels of water vapor can adversely affect the oxidation rate due to competition for adsorption sites [12,13]. As the toluene concentration increases, this competition effect becomes less significant and increasing the water vapor becomes more favorable [12,14,15]. The presence of water vapor seems to also decrease the extent of catalyst deactivation encountered during toluene PCO, more likely due to the greater conversion of toluene to CO_2 in the presence of water vapor rather than to more persistent intermediates as shown by Ibusuki and Takeuchi [16]. Accordingly, the objective of this study was twofold: test the steady-state performance of the proposed STCs for the removal of VOCs using toluene as the target VOC contaminant due to its persistent nature in the environment and low steady-state reactivity during PCO using Degussa P25 [3,17], and examine the influence of water vapor and space time on toluene conversion.

2. Experimental

2.1. Silica–titania composites (STCs) synthesis and characterization

The STCs were prepared by a sol–gel method using tetraethylorthosilicate (TEOS) as the silica precursor. 115 mg of Degussa P25 TiO_2 were added per mL of TEOS present in a mixture consisting of nanopure water, ethanol (Fisher Scientific, 100%), TEOS, 1 M nitric acid (Fisher Scientific, certified ACS), and 3%$_v$ hydrofluoric acid in volume ratios of 12:6.25:9.25:1:1, respectively, to obtain STCs containing approximately 30%$_{wt}$ TiO_2. The suspension was allowed to mix for 20 min before being transferred to assay plates for aging and drying using previously described procedures [18] to produce cylindrical shaped STCs. The STCs were analyzed using N_2 adsorption–desorption isotherms obtained in a Quantachrome Autosorb 1C-MS gas sorption analyzer to characterize the composites for their BET surface area (SA), total pore volume, average pore size, and pore size distribution (PSD). The available TiO_2 SA in the composites was also analyzed by using a novel functionalization procedure described by Marugan et al. [19]. The digested titania samples resulting from this procedure were analyzed for their titanium and phosphorus content using an ICP-AES (PerkinElmer Plasma 3200).

2.2. Annular packed-bed reactor

The reactor and setup used for carrying out the experimental runs are illustrated in Fig. 1. A Pyrex annular reactor of 25 mm annulus with a 25 mm quartz envelope placed at the center of the reactor was packed with STCs to produce heights of approximately 4–8 cm, corresponding to about 65 g and 130 g of STCs, respectively. A porous glass frit at the bottom of the cylindrical reactor served as bed and envelope support. The STCs were packed on top of glass beads to improve gas distribution before reaching the catalyst. The porosity of the packed bed, determined by dividing the

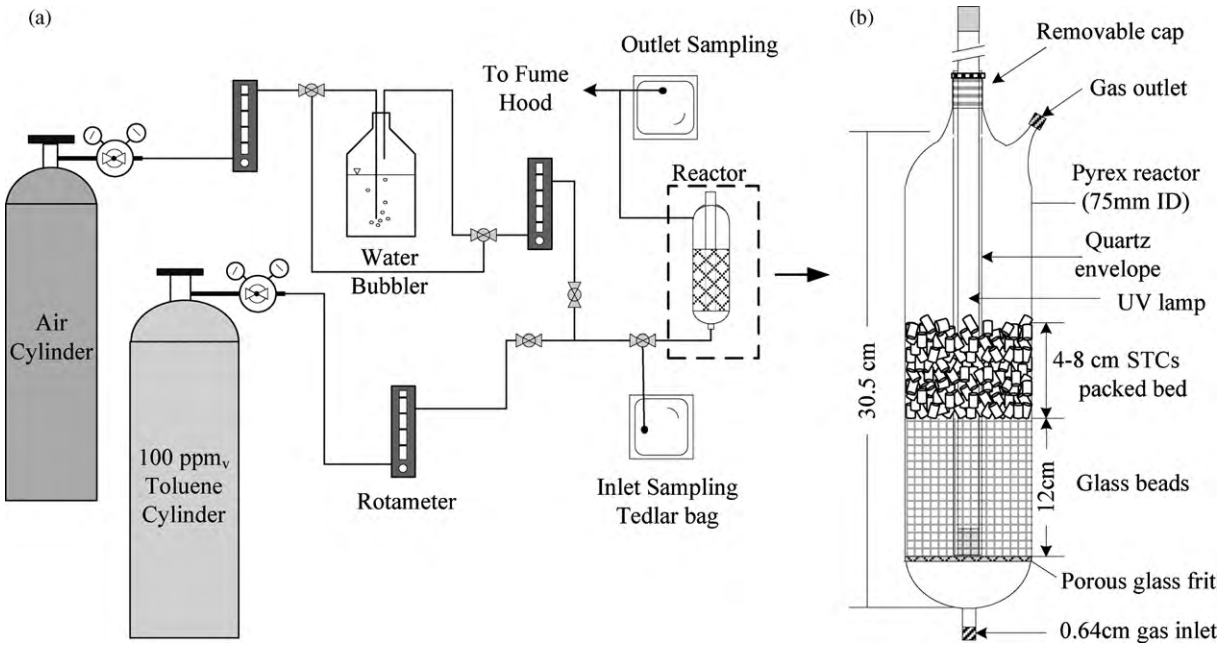

Fig. 1. (a) Schematic of the experimental setup. (b) Photocatalytic packed-bed reactor.

volume of the voids in the packed section by the empty volume of the same section, was about 0.40. A 75 W non-ozone producing UV lamp emitting UV-C radiation with a peak at 253.7 nm (Phillips, TUV 64T5 4P SE UNP) was placed inside the quartz envelope. This lamp was specifically selected to avoid the conversion of toluene that could result from extraneous factors such as ozone forming potential. The intensity, measured using a digital UVX radiometer connected to a 254 nm sensor (UVP, Model UVX-25), at the outside wall of the envelope was 15 mW cm^{-2} while the intensities measured through the packing were 91 μW cm^{-2} at 12.5 mm and 1.7 μW cm^{-2} at 25 mm away from the outside wall of the quartz envelope.

During a typical run, toluene from a compressed cylinder (Airgas, 100 ppm$_v$ Certified Standard) was diluted by mixing with air from another compressed cylinder (Airgas, Breathing Air Standard) to a concentration of 29.4 ± 1.2 mg m^{-3} (~8 ppm$_v$). The desired relative humidity (RH) was achieved by bubbling the air through a flask containing deionized (DI) water before mixing with toluene. The investigated range of RH at room temperature of 23 ± 2 °C varied from 13%, obtained by bypassing the water bubbler, to 90%. The inlet and outlet RH and temperatures were measured using a Hygro-thermometer (EXTECH Instruments, 45320) and the temperatures inside the reactor and at the lamp envelope were monitored with thermocouples. During PCO experiments, no adsorption was allowed to take place before turning the lamp on unless specified, so the results show the combined effects of adsorption and PCO. For PCO experiments, the lamp and reactor were allowed to warm up for at least 1 h before starting the contaminated gas feed until they reached steady-state temperatures corresponding to 50 ± 3 °C inside the reactor and 83 ± 2 °C at the lamp envelope. The gas flowrate (Q) was varied to investigate the effects of superficial velocity (ν) and space time (τ), which were determined using Eqs. (1) and (2), respectively:

$$\nu = \frac{Q}{A} \quad (1)$$

$$\tau = \frac{V}{Q} \quad (2)$$

where A is the cross-sectional area of the reactor normal to the flow (cm^2) and V is the volume of the reactor (cm^3). The flowrates ranged from 12.5 to 26.7 cm^3 s^{-1}, which produced superficial velocities of 0.32–0.68 cm s^{-1} and space times of 5.8–25.0 s, depending on the depth of the packing used. The experiments were run for several hours after steady-state conditions were achieved in the effluent. Influent and effluent samples were collected at different time intervals using 1 L tedlar bags (SKC Inc.) and analyzed the same day. Control experiments were performed in the absence of the catalyst to ensure that toluene did not undergo photolysis or other losses such as adsorption to the systems' appurtenances.

2.3. Analytical methods

All samples were analyzed for toluene by a gas chromatograph (ThermoQuest Trace) equipped with a mass spectrometry (MS) detector (MDL = 0.01 mg m^{-3}) following USEPA Method 524.2 [20]. Some of the potential byproducts reported in the literature that were monitored using the GC/MS included benzene, benzaldehyde and phenol [21,22]. Possible intermediates adsorbed to the catalyst were desorbed from the STCs by placing the crushed catalyst in acetonitrile for 1 h. The suspension was separated using 0.45 μm cellulose acetate filters and the solution was analyzed using HPLC [23].

Table 1
Physicochemical properties of silica–titania composites (STCs).

Property	Units	Value ± STD
Diameter	mm	9.1 ± 0.4
Length	mm	8.1 ± 1.1
TiO_2 loading	wt%	29.6 ± 1.4
BET surface area	m^2 g^{-1}	226.3 ± 5.2
Average pore diameter	Å	172.5 ± 10.5
Total pore volume	cm^3 g^{-1}	1.00 ± 0.18

3. Results and discussion

3.1. STCs characterization

The average physicochemical properties and standard deviation (STD), based on at least two measurements, of the STCs used in this study are shown in Table 1. The diameter and length of the cylindrical shaped STCs were 9.1 and 8.1 mm, respectively while the mean TiO_2 loading was 29.6%$_{wt}$. The STCs had an average pore diameter of approximately 172 Å, surface area of 226 m^2 g^{-1} and pore volume of 1.0 cm^3 g^{-1}. The adsorption–desorption isotherms obtained from the analysis (data not shown) followed a Type IV trend with a H1 hysteresis loop (as defined by the IUPAC [24]). These isotherms are characteristic of mesoporous materials with uniform spheroid particles that tend to be nonporous or possess a narrow pore size range. The narrow pore distribution was confirmed by the PSD analysis shown in Fig. 2; computed with the desorption isotherm data using the method proposed by Barret, Joyner and Halenda (BJH), which assumes cylindrical pore geometry [25]. The PSD is an important characteristic of the composite catalyst material since it can affect the diffusion of toluene in the STCs during adsorption and surface reaction and also the desorption of byproducts after oxidation. The STCs showed a unimodal distribution of pore diameters with more than 95% of the pore volume attributed to pore diameters in the range of 75–200 Å. The peak of the PSD at about 120 Å did not correspond to the measured average hydraulic pore diameter of 172 Å. The BJH method for determining the PSD of the STCs assumes the ideality of perfectly cylindrical pores, and this ideality did not apply to the STCs. In addition, there is also the possibility of the presence of networks within the pellets that are not accounted for by the BJH method.

Other physicochemical properties of composites prepared using a similar formulation as the one in this study is given by Byrne et al. [26]. The main differences between the STCs in their study and those used in this work were the aging and drying procedures, which were extended for the STCs in this work to obtain the large pellet size of 9 mm × 8 mm compared to the powder form of the composite used in their study. Some of the material's characteris-

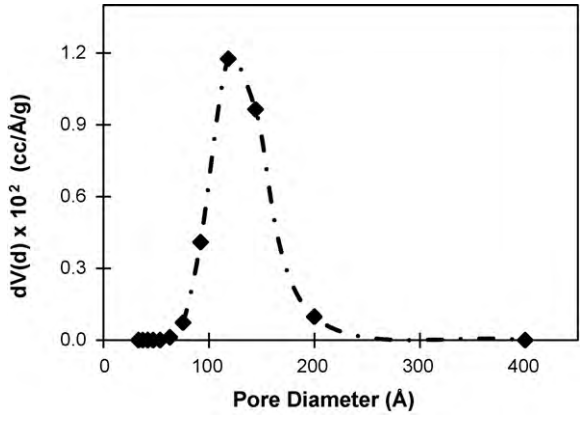

Fig. 2. Pore size distribution of the STC.

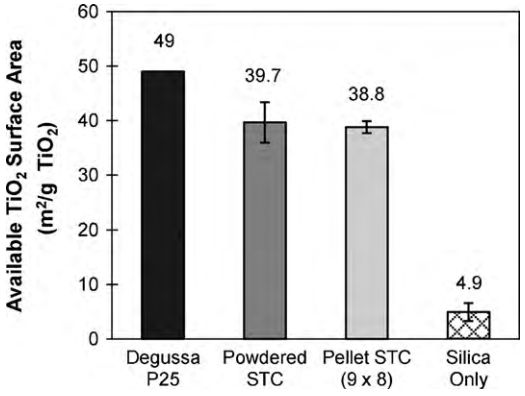

Fig. 3. Available TiO_2 surface area for STCs in the form of powder (powdered STC) and 9 mm × 8 mm cylindrical pellet shape (pellet STC) compared to Degussa P25 and silica only.

tics such as isoelectric point and band gap energy observed by Byrne et al. [26] are expected to apply to these STCs since the highest temperature used during the drying process for this study was 450 °C, which is below the temperatures where TiO_2 phase changes have been observed [27]. However, a main concern about using silica embedded composites and casting them in a large pellet shape was the potential loss of the active catalyst surface area due to entrapment or coating of the TiO_2 when supported by silica and also an increase in mass transfer effects due to the larger pellet size. The latter effects are discussed later in the kinetics section (Section 3.3).

To determine if the activity of the STCs would remain unchanged in the pellet form compared to the powder, the TiO_2 SA available in the composite was analyzed using Marugan et al. [19] functionalization procedure. By this method, the TiO_2 SA that is available for reaction in composites made of both silica and titania can be determined independently from the silica SA. The TiO_2 SA analysis was performed using the STCs in the form of powder (pellets crushed with mortar and pestle), cylindrical pellets (9 mm × 8 mm), and as pellets without any titania loading (silica only). The results for three replicate samples, presented in Fig. 3, indicate that there was about 20–24% loss of TiO_2 SA available for reaction by using silica as the titania support. The decrease in SA can be attributed to possible clumping or coating of the titania particles by silica during the synthesis of the STCs. These results are in agreement with those found by Byrne et al. [26], where approximately 70% of the titania SA was found to be readily available for reaction. However, there were no significant differences in available titania SA between the composites in powder and pellet form, which indicates that the SA of titania available for reaction is not affected by the casting of the STCs as large cylindrical pellets. Based on these results, it is possible to conclude that by extending the aging and drying steps of the STCs synthesis to cast the composites as large pellets that can be used in large-scale systems, the available TiO_2 surface area (i.e. the active photocatalytic component of the STCs) remains unaffected. The very low value found for the "silica only" composites confirms that the method used measures only the functionality of titania so that the contribution of silica to the total active SA can be neglected.

3.2. Photocatalysis of gas-phase toluene

Preliminary experiments showed that significant desorption of toluene occurred when photocatalysis was preceded by adsorption in the dark (data not shown). This was not surprising given the high toluene loading on the STCs during adsorption (about 2.5 mg toluene/g STC at 23 °C and 13% RH) and the large increase in the reactor temperature from approximately 23 °C when the UV lamps were off (during adsorption) to 50 °C after the lamps were turned on (during PCO). Due to the large desorption effect observed when adsorption was followed by PCO, the PCO experiments presented in this work did not include an adsorption step prior to PCO, and so the combined effects of adsorption and PCO are reported. Furthermore, many of the results are presented in terms of the conversion of toluene, which was defined as:

$$\%\text{toluene conversion} = \frac{C_0 - C}{C_0} \times 100 \quad (3)$$

where C_0 is the influent toluene concentration and C is the effluent toluene concentration at any given time. Although many of the potential intermediates such as benzene, benzaldehyde and phenol were monitored during the PCO experiments, neither CO_2 nor total organic carbon concentrations were measured, thus toluene mineralization is not reported, only toluene conversion.

All the experimental runs in this section were performed using a fresh batch of the catalyst pellets, i.e. a virgin catalyst surface, so none of the catalyst was reused or regenerated. At least one replicate experiment was performed for each experimental run. However, given the length of the runs, the sampling was not performed as frequent for the replicate experiments as for the original runs. Nevertheless, the replicate runs ensured that the time to reach steady state and the steady-state concentrations achieved were within a reasonable error (<10%). The experiments were carried out by changing the parameters in a low to high order. For example, for the case where RH was considered, the first experiment performed was at the lowest RH and the last one at the highest RH. Similarly, the experiments considering the effect of space time were performed starting with the lowest space time to the highest time, i.e. decreasing the gas flowrate.

3.2.1. Effect of water vapor on toluene PCO

The effect of water vapor on the removal of toluene by PCO was investigated by increasing the RH from 13% to 90%, which corresponded to water vapor concentrations of about 3600 ppm_v (2600 mg m^{-3}) and 24,500 ppm_v (18,500 mg m^{-3}), respectively. C_0 and τ were kept constant during the experiments at about 30 mg m^{-3} and 12.5 s. The low (13%) and high (90%) RH values were selected since there is evidence in the literature that effects are more pronounced at the extremes of the relative humidity scale [11,14]. Furthermore, the titania immobilization technique used in this work is intended for large-scale systems where controlling a specific RH value might be challenging and costly. In such systems, either dehumidifying the influent stream or completely humidifying it, whichever is more favorable for the conversion, would be more practical than keeping the humidity set at a specific value.

The results showing the effects of RH on toluene conversion are presented in Fig. 4 as a function of run time. Initially, the conversion of toluene was greater than 90% during the first 3.5 h of operation under both low and high RH conditions, likely due to the combined effects of adsorption and PCO. However, under low RH conditions, the conversion of toluene decreased with time to reach a steady-state conversion of about 10%, achieved after 50 h of continuous experimental run. These results are consistent with the decreased photocatalytic activity of Degussa P25 observed by many authors as a function of time for similar C_0 and low RH conditions [11,28,29]. For high RH, steady-state conditions were achieved after only 20 h of operation and the conversion of toluene obtained then was approximately 67%. This conversion remained constant for the following 55 h of the run. Under the same conditions, the steady-state conversion of toluene increased by 57% when the water vapor to toluene ratio was increased by a factor of about 7. Similar to other findings in the literature, these results indicate that increasing the amount of water vapor in the system results in greater conversion of toluene present in the ppm_v range [12,14,30]. Furthermore, these results show that the large difference in conversion of toluene

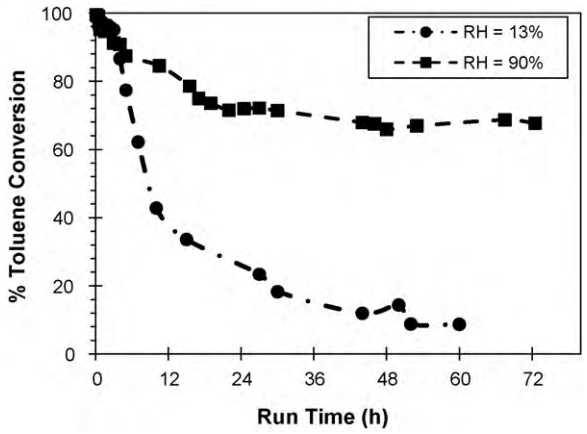

Fig. 4. Toluene conversion as a function of run time for different relative humidity (RH) values. $C_0 = 30\ mg\ m^{-3}$, $\tau = 12.5\ s$, $Z = 4\ cm$.

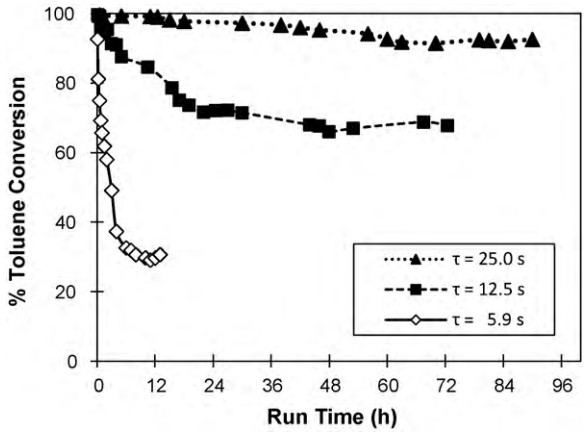

Fig. 5. Toluene conversion as a function of run time for various space times (τ). $C_0 = 30\ mg/m^3$, RH = 90%.

due to RH was not only observed at the beginning of the run, but it was maintained at steady state even after 3 days of continuous operation.

The increase of water vapor in the system helped maintain the catalyst activity for long periods of time. It is important to note however, that the yellowish coloration of the catalyst, commonly attributed to catalyst deactivation, was observed for both low and high RH conditions, despite the large concentrations of water vapor in the system. The change in catalyst color was not observed during adsorption only experiments, thus suggesting that the catalyst poisoning taking place during PCO might be attributed to photocatalytic reactions leading to the formation of persistent byproducts or carbon deposits as it has been suggested by others [21,30]. No byproducts were detected by the GC/MS in the effluent flow during any of the experiments, which is not uncommon for concentrations below 80 ppm_v [11]. However, by analyzing the solution of acetonitrile used to soak and wash the used catalyst, benzaldehyde and benzoic acid were the species desorbed from the STCs under both low and high RH conditions.

3.2.2. Effect of space time on toluene PCO

The effect of space time was determined by changing either the flowrate or the depth of the packed bed. For all runs, the toluene inlet concentration and RH were kept constant at about 30 $mg\ m^{-3}$ and 90%, respectively. By increasing the flowrate, the superficial velocity was correspondingly increased. Similarly, the toluene and water vapor loadings were also modified as a result in the change in flowrate. The experimental conditions used for the runs showing the effect of space time are presented in Table 2.

The effect of space time on the oxidation of toluene is shown in Fig. 5. The increase in space time resulted in an increase in toluene conversion. The initially large conversions observed for all runs decreased to a lower value as steady state was reached. The steady-state conversion was achieved faster (within 4 h of the run) for the shorter space time, likely due to the larger toluene and water vapor loadings. For the longest space time of 25.0 s, steady state was reached after about 60 h of operation. The steady-state toluene conversions achieved were approximately 31%, 67% and 93% for the space times of 5.9, 12.5 and 25.0 s, respectively. These results, which are consistent with the trends observed in other studies [5,31,32], are not surprising since increasing the space time of toluene in the reactor provides longer adsorption and contact times, thus increasing the chances of toluene to react with hydroxyl radicals for conversion.

By using high water vapor concentrations and increasing the space time, catalyst deactivation was expected to be overcome. The yellowish coloration of the STCs, however, was observed in all runs, suggesting that some catalyst poisoning was still taking place even after the space time was doubled. Nonetheless, these results showed that despite the change of color of the catalyst, high steady-state toluene removals (~93%) were achieved and maintained for prolonged periods of time using the STCs.

Although an exact comparison with other studies is almost impossible given the differences in configuration and UV irradiation intensity and distribution in the reactors used in the literature, it is possible to elucidate the advantage of the STCs on the conversion of toluene over other immobilization techniques such as wall coating. For example, Jeong et al. [33] used an annular reactor with walls coated with Degussa P25 TiO_2 of comparable volume and operating conditions to the one used in experimental run 3 ($\tau = 25$ s). These authors [33] found initial toluene conversions of about 75% but steady-state conversions of only 10% after 3 h of continuous run for space times of 33 s, λ of 254 nm, C_0 of 10 ppm_v and about 40% RH. Despite the lower RH of the study used for comparison, Obee and Brown [12] and Jeong et al. [15] have shown that for the toluene concentrations selected in the range of 10 ppm_v, the oxidation rate of toluene remains relatively constant as long as the RH is greater than about 40%. The large difference in steady-state conversions of toluene (about 83% greater in this study) might be mostly attributed to the greater amount of TiO_2 per volume of reactor (about 1000

Table 2
Summary of experimental conditions to assess the effect of space time on toluene conversion.

Parameters	Unit	Experimental run		
		1	2	3
τ	s	5.9	12.5	25.0
Z	cm	4	4	8
Q	cm^3/s	26.7	12.5	12.5
V	cm/s	0.68	0.32	0.32
Toluene loading rate	mg/min	0.048	0.022	0.022
Water vapor loading rate	mg/min	31.5	14.5	14.5

Table 3
Toluene oxidation rate and Mears (C_M) and Weisz-Prater (C_{WP}) Criteria for the determination of mass transfer influences at various space times.

τ (s)	$-r$ ($\times 10^{11}$ mol g_{STC}^{-1} s^{-1})	$-r'$ ($\times 10^{5}$ mol s^{-1} m^{-3})	k_c ($\times 10^{3}$ m s^{-1})	$C_M < 0.15$ at $C_b = C_0$	$C_{WP} < 1$ at $C_b = C_0$
5.9	4.17	1.73	2.5	0.049	0.27
12.5	4.07	1.69	1.6	0.077	0.26
25.0	2.84	1.18	1.6	0.051	0.18

times greater in this study) and also the enhanced adsorption capacity provided by the silica supports, which are major advantages of the STCs when considered for large-scale applications.

3.3. Kinetic analysis

The kinetic analysis was performed using the steady-state results from the experiments described in Table 2. Kinetic data free of mass transfer influences can be better analyzed than in the presence of mass transfer limitations. Resistance to mass transfer can be either external, from the bulk phase to the catalyst pellet, or internal, which refers to the diffusion through the pores. External mass transfer influences are usually assessed by increasing the flowrate in the reactor since it is well established that in the presence of external mass transfer influences, the reaction rate increases with fluid velocity. If the system is free of external mass transfer influences, the oxidation rate will be the same despite the increase in superficial velocity. The average rate of reaction (r) used to determine the influence of external mass transfer on toluene oxidation was calculated by Eq. (4):

$$-r = Q\frac{dC}{dW} = \frac{Q}{W}(C_0 - C_e) \tag{4}$$

where C_e is the effluent toluene concentration obtained at steady state and W is the weight of the STCs. These reaction rates are shown in Table 3. For the two cases where the superficial velocity was increased by increasing the flowrate and keeping the same packed volume, the reaction rates were very similar, 4.17×10^{-11} and 4.07×10^{-11} mol s^{-1} g_{STC}^{-1}. Based on these values, it is expected that external mass transfer influences were not significant. However, when the reactor used to make this comparison is not a differential reactor, such is the case in this study, the intrinsic rate of reaction might also be affected by the increase in flowrate due to the larger differences between inlet and outlet concentrations, making it hard to differentiate the two effects, unless the studies are performed using two different catalyst beds with the same space time and different velocities [34]. This case was not investigated in this work. Therefore, to further determine if the external mass transfer resistance was significant, the Mear's criterion (C_M) was used [35]. This criterion uses the measured rate of reaction (r) to determine if the external mass transfer can be neglected. The Mears criterion states that when the inequality shown in Eq. (5) is satisfied, external mass transfer effects are negligible. The variables in C_M include the characteristic pellet radius R (radius/2 for cylindrical pellets), the reaction order n (assumed to be 1 for toluene), the mass transfer coefficient k_c, which was determined using Colburn J factor mass transfer correlations, and the bulk concentration C_b [35].

$$C_M = \frac{-r \times R \times n}{k_c \times C_b} < 0.15 \tag{5}$$

The calculation results for the Mears' criterion, shown in Table 3, indicate the criterion is satisfied ($C_M < 0.15$) for all flow conditions investigated when C_b is assumed to be the same as C_0. Since this assumption is not certain, the minimum C_b required to meet the criteria was determined. The bulk concentrations should be above 2.5, 3.9 and 2.6 ppm_v for experimental runs 1, 2 and 3, respectively if the criterion is to be met. Given that these concentrations are less than half the initial concentrations, it is possible to conclude that the criteria will be satisfied for most of the concentrations encountered in the system. Accordingly, external mass transfer resistances can be neglected and it can be assumed that there are no concentration gradients between the bulk and the external surface of the catalyst pellets.

Similarly, the influences of internal mass transfer in the kinetics of the reaction were assessed by using the Weisz-Prater Criterion (C_{WP}). When the inequality for the Weisz-Prater criterion described by Eq. (6) holds, it means that pore diffusion is not important in the system and can be neglected. This criterion is also a function of R, C_b (in this case assumed to be the same as C_0 due to the lack of external mass transfer limitations found above), the density of the catalyst pellet (ρ_c) and the effective diffusivity (D_e) [35].

$$C_{WP} = \frac{-r \times \rho_c \times R^2}{D_e \times C_b} < 1.0 \tag{6}$$

The effective diffusivity, defined by Eq. (7), is a function of the diffusivity (D) of the contaminant in the gas phase ($D = 7.55 \times 10^{-6}$ m^2 s^{-1}, used for toluene diffusivity in air [36]), the catalyst grain porosity (ε), determined to be 0.7 for the STCs used in this study, and the tortuosity factor for the STCs (τ_c), which was assumed to be 3, as it usually is for many mesoporous materials [34].

$$D_e = \frac{D \times \varepsilon}{\tau_c} \tag{7}$$

The values obtained from the Weisz-Prater expression for the different flow conditions used in the experimental runs are shown in Table 3. All these values are less than 1, meaning that there are no diffusion limitations inside the pellets and consequently no concentration gradients within in the STCs.

Based on the Mears and Weisz-Prater criteria, the measured rates of reaction at steady state can be considered free of mass transfer influences, so they are expected to be the result of the intrinsic kinetics only. Consequently, the steady-state removals at various space times shown in Fig. 5 were used to determine the reaction rate constant for toluene oxidation using the STCs. The Langmuir–Hinshelwood (L–H) model has been successfully used by many researchers to describe and model the degradation rates of toluene PCO using Degussa P25 [12,14,32]. Based on the negligible mass transfer effects previously assessed and assuming that the effect of intermediates formation is negligible, the rate of reaction for a plug flow annular packed-bed reactor can be described by Eq. (8):

$$r = -Q\frac{dC}{dV} = \frac{kKC}{1 + KC} \tag{8}$$

where k is the rate constant and K is the adsorption equilibrium constant. For low inlet contaminant concentrations ($KC \ll 1$), the L–H kinetic equation can be reduced to a pseudo-first-order rate equation, with an overall rate constant k' equal to kK, shown by Eq. (9).

$$\ln\left(\frac{C_0}{C}\right) = k'\tau \tag{9}$$

The experimental results for the L–H model are presented in Fig. 6. The L–H model resulted in a good fit of the data ($R^2 > 0.99$), indicating that the kinetic step seems to be the limiting step and

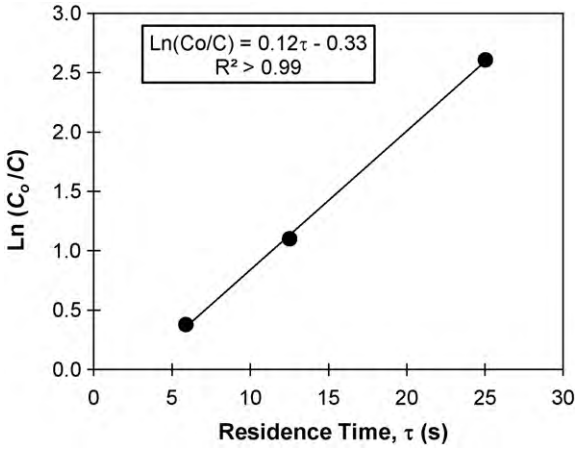

Fig. 6. Linear regression of the Langmuir–Hinshelwood model assuming low influent toluene concentration.

the assumptions about the mass transfer influences were properly assessed. The rate constant determined from the slope of the linear regression equation fit in Fig. 6 was 0.12 s^{-1}. Stokke and Mazyck [10], who used a similar STCs formulation for the removal of methanol, found in their kinetics analysis a rate constant of 0.40 s^{-1} for methanol. This k' is larger than the rate constant found for toluene in this study. Similarly, other researchers investigating the PCO of various VOCs have also found rate constants for alcohols that are higher than those of aromatics under the same operating conditions [14,37]. This can be expected given the structure of the molecules. Aromatic compounds have a benzene ring which tends to be harder to break down during oxidation. Alcohols, on the other hand, tend to be smaller molecules with an OH terminal group that is usually very reactive.

4. Conclusions

The photocatalytic oxidation of toluene in a reactor packed with silica–titania composites (STCs) suitable for large-scale applications was studied. The STCs were analyzed for their available TiO_2 surface area (SA). It was determined that by using silica as the support for TiO_2, a maximum of 24% of the expected titania SA was lost, but no further losses of TiO_2 were found by casting the hybrid composites as large cylindrical pellets. The conversion of toluene was investigated as a function of two important parameters, RH and space time. Both of them influenced the conversion of toluene dramatically. Increasing the RH from 13% to 90% resulted in an increase in conversion from 10% to 67% at steady state. Longer space times resulted in greater removals, up to 93% for the longest time used of 25.0 s. Catalyst poisoning occurred for all conditions studied, i.e. the STCs turned yellowish despite the operating conditions of the experiments. However, unlike many other studies on toluene PCO, the poisoning did not cause complete deactivation of the catalyst since large steady-state removals were still observed after prolonged periods of time. The L–H model simplified to a pseudo-first-order reaction rate equation resulted in a good fit of the kinetics data, with a rate constant of 0.12 s^{-1}. The results of this study support that the STCs can effectively remove toluene from air streams and that high conversion (>90%) can be achieved and maintained using short space times despite the initial poisoning of the catalyst.

Acknowledgment

The authors are appreciative of NASA-UF ES-CSTC at the University of Florida for sponsoring this work.

References

[1] A.D. Cortese, Environ. Sci. Technol. 24 (1990) 442–448.
[2] U.S. Environmental Protection Agency (USEPA), 40 CFR Parts 50 and 58, National Ambient Air Quality Standards for Ozone: Proposed Rule, Federal Register 75 (2010) 2938–3052.
[3] A.J. Maira, K.L. Yeung, J. Soria, J.M. Coronado, C. Belver, C.Y. Lee, V. Augugliaro, Appl. Catal. B: Environ. 29 (2001) 327–336.
[4] A. Bouzaza, A. Laplanche, J. Photochem. Photobiol. A: Chem. 150 (2002) 207–212.
[5] N. Quici, M.L. Vera, H. Choi, G.L. Puma, D.D. Dionysiou, M.I. Litter, H. Destaillats, Appl. Catal. B: Environ. 95 (2010) 312–319.
[6] R.-B. Zhang, J. Non-Cryst. Solids 351 (2005) 2129–2132.
[7] J. Mo, Y. Zhang, Q. Xu, R. Yang, J. Hazard. Mater. 168 (2009) 276–281.
[8] L. Zou, Y. Luo, M. Hooper, E. Hu, Chem. Eng. Process 45 (2006) 959–964.
[9] J.M. Stokke, D.W. Mazyck, C.Y. Wu, R. Sheahan, Environ. Prog. 25 (2006) 312–318.
[10] J.M. Stokke, D.W. Mazyck, Environ. Sci. Technol. 42 (2008) 3808–3813.
[11] K. Demeestere, J. Dewulf, H. Van Langenhove, Crit. Rev. Environ. Sci. Technol. 37 (2007) 489–538.
[12] T.N. Obee, R.T. Brown, Environ. Sci. Technol. 29 (1995) 1223–1231.
[13] M. Sleiman, P. Conchon, C. Ferronato, J.-M. Chovelon, Appl. Catal. B: Environ. 86 (2009) 159–165.
[14] S.B. Kim, S.C. Hong, Appl. Catal. B: Environ. 35 (2002) 305–315.
[15] J. Jeong, K. Sekiguchi, W. Lee, K. Sakamoto, J. Photochem. Photobiol. A: Chem. 169 (2005) 279–287.
[16] T. Ibusuki, K. Takeuchi, Atmos. Environ. 20 (1986) 1711–1715.
[17] R.M. Alberici, W.F. Jardim, Appl. Catal. B: Environ. 14 (1997) 55–68.
[18] C. Akly, P.A. Chadik, D.W. Mazyck, International Conference on Environmental Systems, Savannah, GA, 2009.
[19] J. Marugán, M.-J. López-Muñoz, J. Aguado, R. van Grieken, Catal. Today 124 (2007) 103–109.
[20] U.S. Environmental Protection Agency (USEPA), in: J.W. Munch (Ed.), Method 524.2: Measurement of Purgeable Organic Compounds in Water by Capillary Column Gas Chromatography/Mass Spectrometry, 1995.
[21] V. Augugliaro, S. Coluccia, V. Loddo, L. Marchese, G. Martra, L. Palmisano, M. Schiavello, Appl. Catal. B: Environ. 20 (1999) 15–27.
[22] R. Méndez-Román, N. Cardona-Martínez, Catal. Today 40 (1998) 353–365.
[23] G. Marcì, M. Addamo, V. Augugliaro, S. Coluccia, E. García-López, V. Loddo, G. Martra, L. Palmisano, M. Schiavello, J. Photochem. Photobiol. A: Chem. 160 (2003) 105–114.
[24] K.S.W. Sing, D.H. Everett, R.A.W. Haul, L. Moscou, R.A. Pierotti, J. Rouquerol, T. Siemieniewska, Pure Appl. Chem. 57 (1985) 603–619.
[25] E.P. Barrett, L.G. Joyner, P.P. Halenda, J. Am. Chem. Soc. 73 (1951) 373–380.
[26] H.E. Byrne, W.L. Kostedt Iv, J.M. Stokke, D.W. Mazyck, J. Non-Cryst. Solids 355 (2009) 525–530.
[27] J. Zhang, M. Li, Z. Feng, J. Chen, C. Li, J. Phys. Chem. B 110 (2006) 927–935.
[28] O. d'Hennezel, P. Pichat, D.F. Ollis, J. Photochem. Photobiol. A: Chem. 118 (1998) 197–204.
[29] M. Lewandowski, D.F. Ollis, Appl. Catal. B: Environ. 45 (2003) 223–238.
[30] H. Einaga, S. Futamura, T. Ibusuki, Environ. Sci. Technol. 35 (2001) 1880–1884.
[31] C.H. Ao, S.C. Lee, C.L. Mak, L.Y. Chan, Appl. Catal. B: Environ. 42 (2003) 119–129.
[32] A.K. Boulamanti, C.A. Korologos, C.J. Philippopoulos, Atmos. Environ. 42 (2008) 7844–7850.
[33] J. Jeong, K. Sekiguchi, K. Sakamoto, Chemosphere 57 (2004) 663–671.
[34] C. Satterfield, Mass Transfer in Heterogeneous Catalysis, MIT Press, Cambridge, MA, 1970.
[35] H.S. Fogler, Elements of Chemical Reaction Engineering, Prentice Hall PRT, Upper Saddle River, NJ, 1999.
[36] Landolt-Börnstein IV/15A, Chapter 5.1.1: Diffusion of Gas/Vapor in Gas; doi:10.1007/978-3-540-49718-9_832.
[37] A. Bouzaza, C. Vallet, A. Laplanche, J. Photochem. Photobiol. A: Chem. 177 (2006) 212–217.